Supporting Information

Huang et al. 10.1073/pnas.1506488112

SI Materials and Methods

Mice. PSD-95 KO mice and littermate controls of either sex were generated from heterozygous breeding pairs from a mixed 129SV/C57Bl6 background and housed in cages (33 × 17 cm) of maximally five mice with a 12-h light/dark cycle and food and water ad libitum (1, 2). Genotypes were determined by PCR with the primer pair CAGGTGCTGCTGGAAGAAGG and CTACCCTGTGATCCAGAGCTG to detect both the WT and KO allele with sizes of 255 and 355 bp, respectively. To identify PV+ interneurons, a PV-Cre driver line and an YFP reporter mouse line were crossed into the PSD-95 mouse line (3, 4). All procedures were performed in the light cycle by strictly following the procedures approved by the animal care and use committees and governmental agencies of the listed institutions.

Visual Cortex Slice Preparation. Coronal visual cortical slices (300 μm) from juvenile and adult (*Results*) mice were sliced with a vibratome in ice-cold sucrose (in mM: sucrose 168, NaCl 25, KCl 1.9, $MgSO_4$ 10, $NaHCO_3$ 26, NaH_2PO_4 1.2, D-glucose 25) or *N*-methyl-D-glucamin (NMDG) cutting buffer (in mM: NMDG/HCl 135, KCl 1, $MgCl_2$ 1.5, choline HCO_3 20, KH_2PO_4 1.2, D-glucose 10, $CaCl_2$ 0.5). Slices were recovered at 35 °C for 20 min in standard artificial cerebrospinal fluid (ACSF) [in mM: NaCl 119, $NaHCO_3$ 26, D-glucose 20, KCl 2.5, NaH_2PO_4 1, $MgSO_4$ 1.3, $CaCl_2$ 2.5, saturated with carbogen, 95% (vol/vol) O_2 and 5% (vol/vol) CO_2] and then stored in carbogenated ACSF at room temperature until further use.

Electrophysiology. Standard whole-cell voltage-clamp recordings were carried out at 31–32 °C in a recording chamber, which was perfused (2 mL/min) with ACSF. L2/3 pyramidal neurons were visually identified with infrared-differential interference contrast microscopy. Glass pipettes (2–5 MΩ) were filled with Cs-based internal solution (in mM: $CsMeSO_3$ 117.5, Hepes 10, CsCl 17.8, TEA-Cl 10, EGTA 0.25, D-glucose 10, $MgCl_2$ 2, Na-ATP 4, Na-GTP 0.3, pH7) to record A/N ratios and for the failure analysis and a low Cl^- internal solution (in mM: $CsMeSO_3$ 133, Hepes 10, TEA-OH 10, EGTA 0.25, D-glucose 10, $MgCl_2$ 2, QX314-Cl 5, Na-ATP 4, Na-GTP 0.3, pH7) to record AMPA, NMDA, and GABA-A receptor synaptic currents, evoked with bipolar electrodes placed in L4. The input and series resistance were monitored throughout the recording by applying a short hyperpolarizing voltage step before synaptic stimulation. Only cells with a series resistance smaller than 30 MΩ and changes of series and input resistance of less than 20% were used for analysis. Axons were stimulated in L4 with theta-glass bipolar electrodes, filled with ACSF. Data were filtered at 3 kHz and collected with custom routines in Igor (Wavemetrics), using an ELC-03XS amplifier (NPI) and digitized at 10 kHz with an ITC-18 (HEKA). Glutamatergic transmission was isolated pharmacologically with 50 μM picrotoxin-supplemented ACSF, and polysynaptic activity was prevented in A/N ratio recordings with 1 μM 2-chloroadenosine if necessary; 10 μM NBQX was supplemented to block AMPA receptors. mEPSCs were recorded in the presence of 0.5 μM TTX to block action potentials, and events were analyzed with Minianalysis (Synaptosoft).

Synaptic Failure Analysis. The stimulation strength was adjusted such that ∼50% of the trials elicited unitary AMPA receptor responses at a $V_h = -60$ mV (Figs. 3 and 5). At a $V_h = +40$ mV, we then measured a composite response mediated by AMPA and NMDA receptors. Percent silent synapses were calculated using Eq. **S1**

$$-\ln(F_{-60})/\ln(F_{+40}) \quad \textbf{[S1]}$$

in which F_{-60} was the failure rate at −60 mV and F_{+40} was the failure rate at +40 mV (5, 6).

AAV Transduction. The EGFP cDNA was introduced after the CAG promoter in an AAV expression vector, which resulted in the AAV-GFP (7). The 5′ of the CAG promoter and the sh95 expression cassette, driven by the human U6 promoter, were shuttled from a lentiviral expression construct to result in the bicistronic AAV-sh95 (8). A control AAV was constructed, which expressed an shRNA against luciferase (shLC; Addgene 26701). AAVs were produced according to described procedures, pseudotyped with the capsid for AAV8, and purified by iodixanol gradient centrifugation (9). For P0 mice AAV delivery, P0–P1 mouse pups were anesthetized on ice for 5 min and immobilized with a holder on the injection table, where the surface temperature was kept at 4 °C. The intersection of the sagittal and the lambdoid suture (lambda) was visually identified through the skin. Injections of AAV (13.4 nL each, 23 nL/s) were delivered at two positions bilaterally into V1 (from lambda, in mm: AP +0.1, ML ±1.25, DV −0.8 and AP +0.3, ML ±1.8, DV −0.8) using a glass capillary with a Nanoject II microinjector (Drummond). For P40 mice AAV delivery, animals were anesthetized with a mixture of fentanyl (0.07 mg/kg), midazolam (7.0 mg/kg), and medetomidin (0.7 mg/kg), and the head was fixed on a stereotaxic apparatus (Stoelting); 0.5 μL AAV (100 nL/min) was injected at two positions bilaterally into V1 (from Bregma, in mm: AP −3.8, ML ±2.4, DV −1.6 and AP −2.8, ML ±3.0, DV −1.4) using a glass pipette controlled by a Microsyringe pump controller (WPI).

Confocal Image Analysis. Under isoflurane anesthesia, mice were transcardially perfused with 70 mL ice-cold PBS, followed by 70 mL ice-cold 4% paraformaldehyde in PBS. Brains were collected and postfixed with 4% paraformaldehyde for 10 min, followed by three incubations in PBS. Brain slices (300 μm) including V1 were prepared in PBS by a vibratome. After three incubations (1 min) in PBS, slices were incubated with 3 μg/mL DAPI for 10 min. After an additional PBS incubation, they were mounted on glass slides. Confocal images were acquired with a Carl Zeiss LSM 710 microscope with a 10× objective and a resolution of 2,048 × 2,048 pixels. Imaging parameters were maintained constant for acquisition of different experimental conditions.

Subcellular Fractionation. Subcellular fractions with enriched PSD from PSD-95 KO and littermate WT control mice were prepared as described previously (8). One mouse cortex without hippocampus was homogenized in 10 volumes of homogenization buffer (4 mM Hepes/NaOH, pH 7.4, 320 mM sucrose; Fig. S2). A crude synaptosomal pellet (P2) was isolated by differential centrifugation and was resuspended in resuspension buffer [in mM: NaF 50, Hepes/NaOH 50, pH 7.4, EDTA 1, $NaVO_4$ 0.2, and complete protease inhibitors (Roche) 1 μg/μL]. Samples were extracted with 0.5% Triton X-100 for 15 min and then centrifuged 20 min at 32,000 × *g* to obtain the Triton insoluble (1TP) and soluble (1TS) fraction. The pellet was resuspended in half of the previous volume of the resuspension buffer and extracted in 3% *N*-lauroylsarcosine for 10 min. The extract was centrifuged for 1 h at 200,000 × *g* to obtain the *N*-lauroylsarcosine insoluble (TSP) PSD and soluble (TSS) fraction. All fractions were protected against proteolysis with 1% SDS and adjusted to 1 μg/μL in the SDS sample buffer.

Antibodies and Quantitative Western Blotting. Ten to 30 μg protein on different gels but similar amounts per lane were separated on Bis-Tris polyacrylamide gels and transferred onto nitrocellulose membranes (8). Protein bands were decorated with the following primary antibodies: $GABA_A$ receptor-α1, SAP102, PSD-95, mortalin, GluA2, GluN2B (mouse; University of California Davis/National Institutes of Health NeuroMab), Rab3A, Synaptophysin (mouse; Synaptic Systems), GluN2A, GluA1 (rabbit; Millipore), GluA3, GluA4 (rabbit; Abcam), and gephyrin (mouse; Synaptic Systems). Bands were detected by the secondary antibodies goat anti-mouse Alexa 680 (Invitrogen), goat anti-rabbit Alexa 680 (Invitrogen), goat anti-mouse IR800 (Li-COR Biosciences), and goat anti-rabbit IR800 (Li-COR Biosciences), visualized, and quantified with an infrared fluorescence scanner.

VWT. The visual acuity of the mice was assessed using the VWT, a visual discrimination task that is based on reinforcement learning (10, 11). For this task, mice were initially trained to distinguish a low spatial frequency vertical sine wave grating (0.086 cycles/deg) from isoluminant gray, and then their ability to recognize higher spatial frequencies was tested. The apparatus consisted of a trapezoidal-shaped water-filled pool with two monitors placed side by side at one end (Fig. S1). An escape platform that was invisible to the mice was placed below the monitor on which the rewarded stimulus (grating) was projected. The position of the grating and the platform was alternated in a pseudo-random sequence over the training and test trials. Once 90% accuracy was achieved, the discrimination threshold was determined by increasing the spatial frequency of the grating until performance falls below 70% accuracy. The highest spatial frequency at which 70% accuracy was achieved was taken as the maximum visual acuity.

MD. The right eye was deprived of vision for 4 or 7 d according to published protocols (12, 13). Briefly, mice were anesthetized with 2% isofluorane in 1:1 O_2:N_2O. Lid margins were trimmed, and an antibiotic gel (gentamicin) was applied. The eye was closed with two mattress sutures. Mice were checked daily to make sure that the eyes remained closed. After MD, the mice were returned to their home cages.

Treatment with Diazepam. To increase GABAergic inhibition, we applied diazepam (Rotexmedica; i.p.), an allosteric $GABA_A$ receptor modulator. Injections were performed about 4 h before MD and were continued for 6 d during MD with one injection per day. The dose used (1 mg/kg mouse) was selected as it reliably abolished OD shifts in 3-mo-old WT mice. In addition, it allowed normal activity and exploratory behavior.

Optical Imaging of Intrinsic Signals and Visual Stimuli. After initial anesthesia with 2% halothane in a mixture of 1:1 O_2/N_2O, the mice received atropine (0.15 mg, s.c.; Franz Köhler), dexamethasone (0.2 mg/mouse, s.c.; Ratiopharm), and chlorprothixene (0.2 mg/mouse, i.m.; Sigma). In addition, lidocaine (2% xylocain jelly) was applied locally to all incisions. The mice were placed in a stereotaxic frame, their body temperature was maintained at 37 °C, and electrocardiograph leads were attached to monitor the heart rate throughout the experiment. Anesthesia was maintained with 0.6–0.8% halothane in a mixture of 1:1 O_2/N_2O applied through a tube over the nose. We incised the skin to expose the visual cortex of the left hemisphere. Low-melting point agarose (2.5% in NaCl) and a glass coverslip were placed over the exposed area. To avoid dehydration of the mouse during the experiment, we injected 0.2 mL saline (0.9%, s.c.).

Mouse visual cortical responses were recorded through the skull using the imaging method developed by Kalatsky and Stryker and optimized for the assessment of OD plasticity by Cang et al. (13, 14). The experimenter was blinded for the genotype of the recorded mouse. Briefly, a temporally periodic stimulus was continuously presented to the animal, and the cortical response at the stimulus frequency was extracted by Fourier analysis. Optical images of intrinsic cortical signals were obtained using a Dalsa 1M30 CCD camera controlled by custom software. Using a 135 × 50-mm tandem lens configuration (Nikon), we imaged a cortical area of 6.4 × 6.4 mm^2. The surface vascular pattern and intrinsic signal images were visualized with illumination wavelengths set by a green (550 ± 10 nm) or red (610 ± 10 nm) interference filter, respectively. After acquisition of a surface image, the camera was focused 600 μm below the cortical surface. An additional red filter was interposed between the brain and the CCD camera. Frames were acquired at a rate of 30 Hz temporally binned to 7.5 Hz and stored as 512 × 512 pixel images after spatial binning of the camera image. To display visual stimuli, a high refresh rate monitor [Benq BL240 (LED), 1,920 × 1,080 at 60 Hz] was placed in front of the mouse at a distance of 25 cm with its midline aligned to the animal. Drifting horizontal bars (2° wide) were presented to the animal at a distance of 25 cm on a high refresh rate monitor. For imaging ODP, the visual stimulus was restricted to the binocular visual field of the left primary visual cortex (V1; −5° to +15° azimuth), and mice were stimulated through either the left or the right eye in alternation to assess the OD. For visualizing elevation and azimuth maps, we used full-field stimuli extending 94° horizontally and 62° vertically (Fig. S1) and contralateral eye stimulation.

Data Analysis. Visual cortical maps were calculated from the acquired frames by Fourier analysis to extract the signal at the stimulation frequency using custom software (14). Although the phase component of the signal was used for the calculation of retinotopy, the amplitude component represented the intensity of neuronal activation (expressed as fractional change in reflectance $\times 10^{-4}$) and was used to calculate ocular dominance (13, 15). To quantify OD plasticity, an OD score of each pixel in the binocularly activated region was calculated as $(C - I)/(C + I)$, with C and I representing the raw response magnitudes of each pixel to visual stimulation of the contralateral and ipsilateral eye, respectively. We then computed an ODI as the average of the OD scores of all responsive pixels. Consequently, ODIs ranged from −1 to 1, with negative values representing ipsilateral and positive values representing contralateral dominance. At least three maps per animal were averaged to compute the ODI. The ODIs were color-coded in a 2D map of the OD scores (OD map): cold colors represent negative values (ipsilateral eye dominance) and warm colors represent positive values (contralateral eye dominance; Fig. 1 *A*–*F*).

1. Yao W-D, et al. (2004) Identification of PSD-95 as a regulator of dopamine-mediated synaptic and behavioral plasticity. *Neuron* 41(4):625–638.
2. Abbas AI, et al. (2009) PSD-95 is essential for hallucinogen and atypical antipsychotic drug actions at serotonin receptors. *J Neurosci* 29(22):7124–7136.
3. Hippenmeyer S, et al. (2005) A developmental switch in the response of DRG neurons to ETS transcription factor signaling. *PLoS Biol* 3(5):e159.
4. Madisen L, et al. (2010) A robust and high-throughput Cre reporting and characterization system for the whole mouse brain. *Nat Neurosci* 13(1):133–140.
5. Liao D, Hessler NA, Malinow R (1995) Activation of postsynaptically silent synapses during pairing-induced LTP in CA1 region of hippocampal slice. *Nature* 375(6530):400–404.
6. Isaac JTR, Nicoll RA, Malenka RC (1995) Evidence for silent synapses: Implications for the expression of LTP. *Neuron* 15(2):427–434.
7. Petreanu L, Mao T, Sternson SM, Svoboda K (2009) The subcellular organization of neocortical excitatory connections. *Nature* 457(7233):1142–1145.
8. Bonnet SAD, et al. (2013) Synaptic state-dependent functional interplay between postsynaptic density-95 and synapse-associated protein 102. *J Neurosci* 33(33):13398–13409.
9. Suska A, Lee BR, Huang YH, Dong Y, Schlüter OM (2013) Selective presynaptic enhancement of the prefrontal cortex to nucleus accumbens pathway by cocaine. *Proc Natl Acad Sci USA* 110(2):713–718.

10. Prusky GT, Alam NM, Beekman S, Douglas RM (2004) Rapid quantification of adult and developing mouse spatial vision using a virtual optomotor system. *Invest Ophthalmol Vis Sci* 45(12):4611–4616.
11. Prusky GT, West PW, Douglas RM (2000) Behavioral assessment of visual acuity in mice and rats. *Vision Res* 40(16):2201–2209.
12. Gordon JA, Stryker MP (1996) Experience-dependent plasticity of binocular responses in the primary visual cortex of the mouse. *J Neurosci* 16(10):3274–3286.
13. Cang J, Kalatsky VA, Löwel S, Stryker MP (2005) Optical imaging of the intrinsic signal as a measure of cortical plasticity in the mouse. *Vis Neurosci* 22(5):685–691.
14. Kalatsky VA, Stryker MP (2003) New paradigm for optical imaging: Temporally encoded maps of intrinsic signal. *Neuron* 38(4):529–545.
15. Lehmann K, Löwel S (2008) Age-dependent ocular dominance plasticity in adult mice. *PLoS ONE* 3(9):e3120.

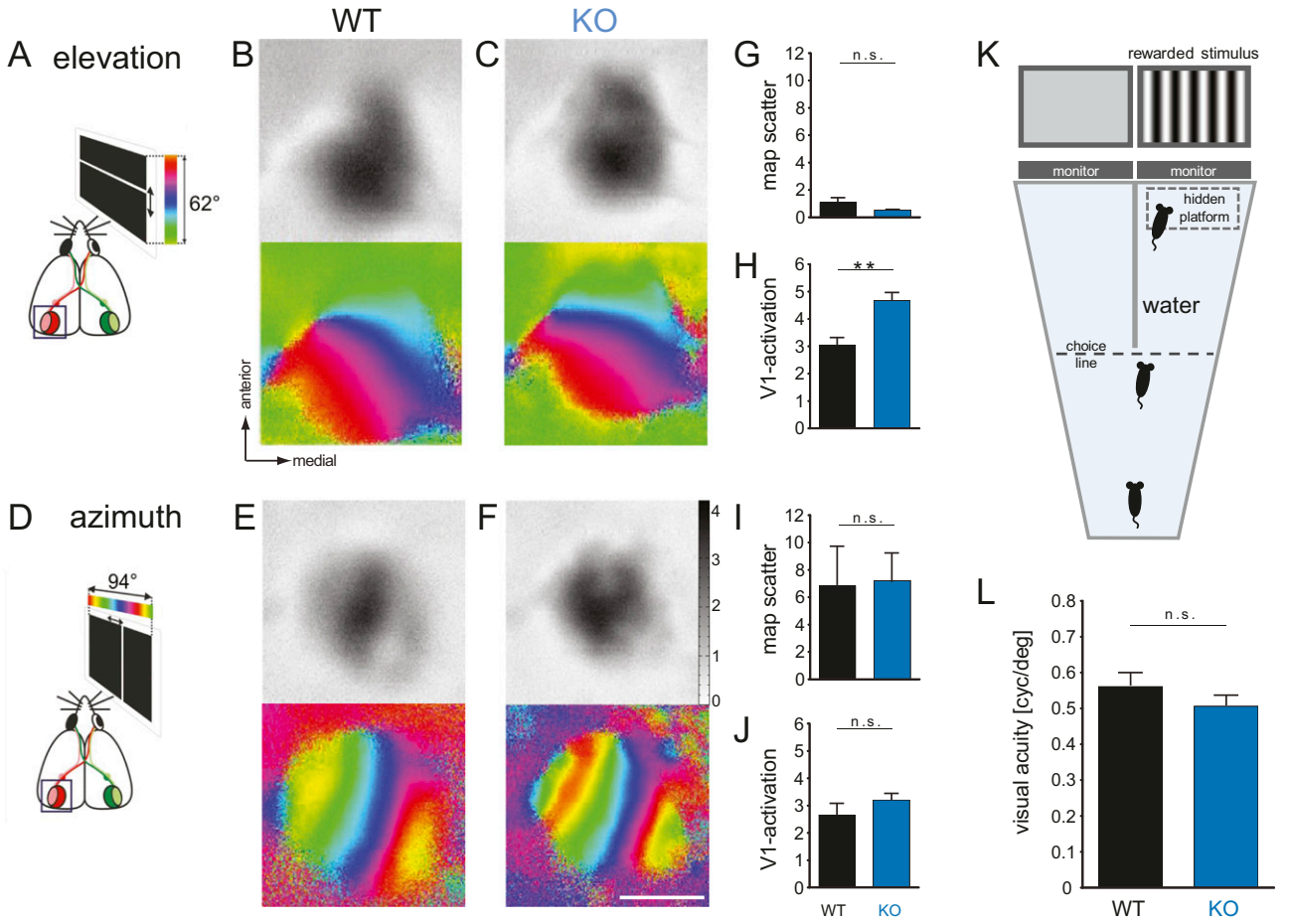

Fig. S1. Normal retinotopic maps and visual acuity in PSD-95 KO mice. (*A–J*) Optically recorded activity and retinotopic maps and their quantification in the left V1 of 3-mo-old WT and PSD-95 KO mice. Both elevation (*B* and *C*) and azimuth maps (*E* and *F*) resulting from visual stimulation of the mice with moving horizontal (*A*) or vertical bars (*D*) are illustrated. Gray-scale coded response magnitude maps (*Upper*) and color-coded phase maps (*Lower*) are shown, together with a quantification of map quality/scatter (*G* and *I*) and V1 activation (*H* and *J*). The magnitude of the optical responses (V1 activation) is expressed as fractional change in reflection $\times 10^{-4}$; the grayscale bar in *F* applies to all amplitude maps. Retinotopic maps are color-coded according to the schemes in *A* and *D*. (Scale bar for all panels with maps, 1 mm.) Note that V1 maps were similar in both genotypes (elevation map scatter: 0.5 ± 0.04 in PSD-95 KOs compared with 1.1 ± 0.32 in WT mice, *t* test, $P = 0.078$; azimuth map scatter: 7.2 ± 2.11 in PSD-95 KOs compared with 6.8 ± 2.87 in WT mice, *t* test, $P = 0.919$; azimuth V1 activation: 3.2 ± 0.23 in PSD-95 KOs compared with 2.7 ± 0.42 in WT mice, *t* test, $P = 0.257$), with the exception of a slightly stronger V1 activation in the elevation maps of PSD-95 KO mice (4.7 ± 0.8 compared with 3.1 ± 0.3 in WT mice, *t* test, $P < 0.01$). (*K* and *L*) Behavioral measurements of visual performance in the VWT. (*K*) Scheme of the VWT apparatus showing the trapezoid water-filled pool, the midline divider, choice line, and the monitors on which visual stimuli are projected. For measuring visual acuity, the mice were trained to swim toward the vertical grating (rewarded stimulus). (*L*) Visual acuity of PSD-95 KO mice was indistinguishable from WT controls (PSD-95 KO: 0.51 ± 0.03 cycles/deg, $n = 8$; WT: 0.56 ± 0.04 cycles/deg, $n = 8$, $P = 0.238$). $^{**}P < 0.01$.

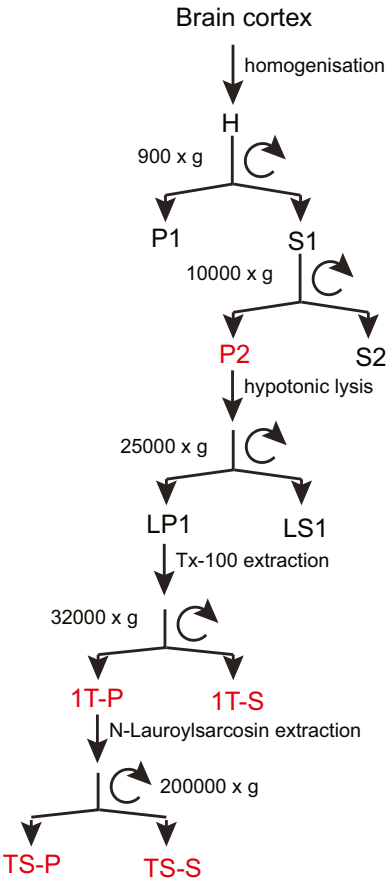

Fig. S2. Subcellular fractionation scheme for the enrichment of PSD proteins. Scheme for the isolation of PSD (TSP) enriched protein fractions. Fractions collected to demonstrate protein enrichment on gel are marked in red.

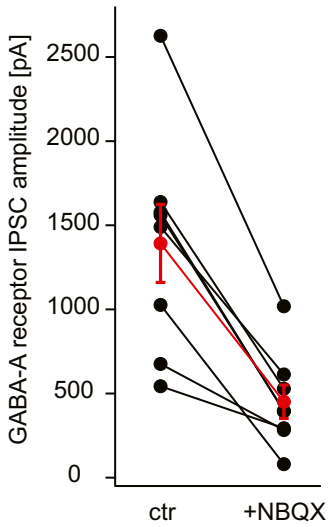

Fig. S3. L4 stimulated IPSCs were primarily bisynaptic. GABAergic IPSCs onto L2/3 pyramidal neurons were evoked by stimulating L4 axons before (ctr) and after wash in of NBQX (+NBQX). IPSCs were isolated by holding the neuron at 0 mV. To measure the level of bisynaptically triggered responses, the AMPA receptor inhibitor NBQX was washed in after 10- to 15-min baseline recording, which resulted on average in a reduction of 68.4 ± 3.4% of the IPSC peak amplitude (in pA: ctr, 1,392 ± 232.3; +NBQX 451.0 ± 99.2).

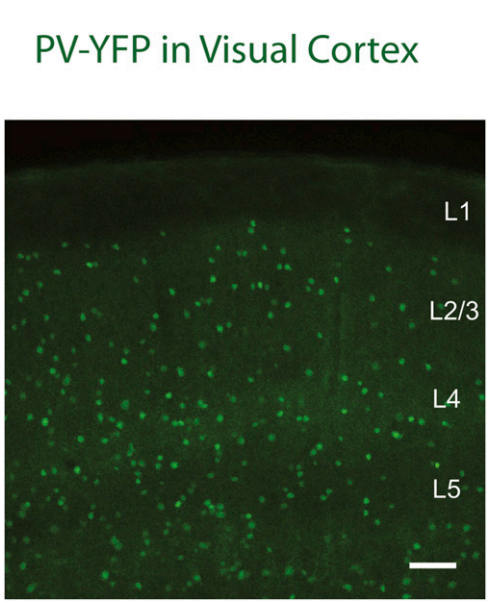

Fig. S4. YFP-labeled PV+ interneurons in V1. Confocal image of the YFP fluorescence of the PV+ reporter mouse, which was used to identify PV+ interneurons in the L2/3 of V1. Cortical layers marked from L1 to L5. (Scale bar, 100 μm.)

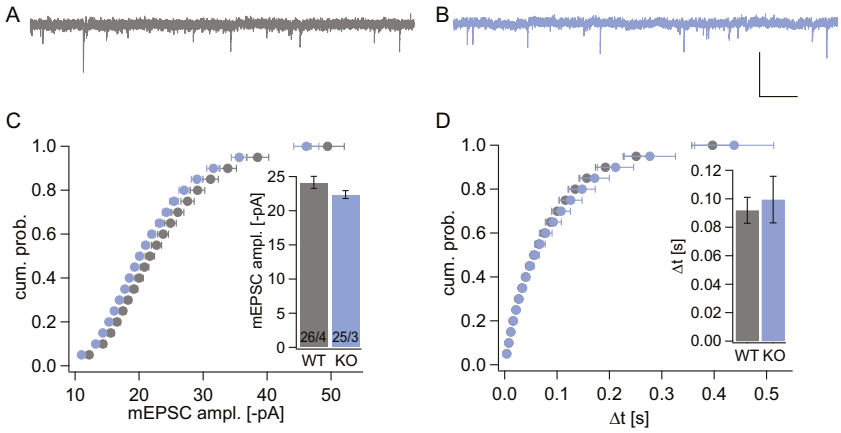

Fig. S5. Analysis of spontaneous synaptic transmission in PV+ interneurons. mEPSCs of PV+ interneurons in L2/3 of V1 were recorded in WT (*A*) and PSD-95 KO (*B*) slices. (*A* and *B*) Sample traces with scale bar 50 pA/100 ms. (*C*) Cumulative probability plot of mEPSC amplitude distribution with 20 bins for peak amplitudes (gray: WT; blue: PSD-95 KO). Average amplitude is plotted in *Inset* with number of cells/number of mice in foot of bar (WT, 24.15 ± 0.88 pA vs. PSD-95 KO, 22.38 ± 0.58, $P = 0.10$). (*D*) Cumulative probability plot and bar graph of average interevent interval in *Inset* of events in *C* (WT, 0.092 ± 0.0092 vs. PSD-95 KO, 0.99 ± 0.016, $P = 0.69$).

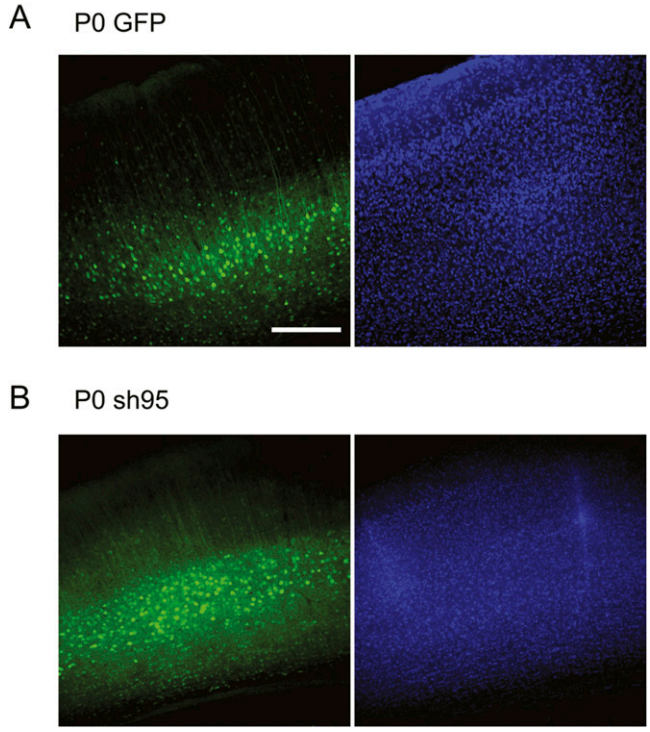

Fig. S6. Analysis of AAV transduction rate. Confocal images of AAV-GFP (*A*) and AAV-sh95 (*B*) of P0 transduced neurons: GFP fluorescence (*Left*) or DAPI fluorescence (*Right*) was captured for cellular level analysis. (Scale bar, 200 μm.)

Table S1. ODIs and V1 activation values of Figs. 1, 6, and 7

		V1 activation	
Group	ODI	C	I
Fig. 1			
WT – no MD	0.30 ± 0.03	1.73 ± 0.16	0.96 ± 0.13
WT <P110 – 7dMD	0.01 ± 0.04	1.76 ± 0.25	1.58 ± 0.17
WT >P110 – 7dMD	0.30 ± 0.02	1.90 ± 0.15	1.05 ± 0.09
KO – no MD	0.32 ± 0.03	2.57 ± 0.18	1.30 ± 0.12
KO <P110 – 7dMD	0.01 ± 0.04	1.18 ± 0.12	1.13 ± 0.16
KO >P110 – 7dMD	0.01 ± 0.02	1.53 ± 0.29	1.41 ± 0.27
KO >P110 – 4dMD	−0.06 ± 0.06	1.26 ± 0.16	1.30 ± 0.13
WT + DZ – MD	0.26 ± 0.03	1.77 ± 0.09	1.13 ± 0.09
KO + DZ – MD	0.00 ± 0.03	1.53 ± 0.17	1.52 ± 0.24
Fig. 6			
GFP P0 – MD	0.28 ± 0.02	1.61 ± 0.27	0.98 ± 0.18
sh95 P0 both – MD	0.01 ± 0.02	0.99 ± 0.13	0.99 ± 0.15
sh95 P0 left – MD	0.05 ± 0.03	1.28 ± 0.21	1.14 ± 0.24
sh95 P0 right – MD	0.24 ± 0.01	1.42 ± 0.16	0.73 ± 0.11
GFP P40 – MD	0.25 ± 0.01	1.50 ± 0.17	0.92 ± 0.10
sh95 P40 – MD	−0.02 ± 0.02	0.86 ± 0.08	0.90 ± 0.10
Fig. 7			
WT – no MD	0.30 ± 0.03	1.73 ± 0.16	0.96 ± 0.13
WT <P110 – 7dMD	0.01 ± 0.04	1.76 ± 0.25	1.58 ± 0.17
WT <P110 2d reopen	0.10 ± 0.03	1.64 ± 0.18	1.30 ± 0.07
WT <P110 4d reopen	0.27 ± 0.01	1.59 ± 0.02	0.91 ± 0.03
KO – no MD	0.32 ± 0.03	2.57 ± 0.18	1.30 ± 0.12
KO <P110 – 7dMD	0.01 ± 0.04	1.62 ± 0.46	1.49 ± 0.39
KO <P110 2d reopen	0.26 ± 0.02	2.02 ± 0.30	1.15 ± 0.13

Table S2. Percentage of silent synapses and AMPA/NMDA EPSC ratio of Figs. 2 and 5

Group	Silent synpases, %	Cells per mice	AMPA/NMDA EPSC ratio	Cells per mice
Fig. 2				
WT P10	55.03 ± 3.82	10/3		
KO P10	55.23 ± 1.53	10/3		
WT P30	26.91 ± 1.53	15/4	1.43 ± SEM (+0.12; −0.11)	19/5
KO P30	49.09 ± 4.27	8/3	1.01 ± SEM (+0.079; −0.073)	19/3
WT P60	7.34 ± 2.65	14/4	2.20 ± SEM (+0.17; −0.16)	14/3
KO P60	46.73 ± 5.14	11/3	1.02 ± SEM (+0.085; −0.078)	13/3
Fig. 5				
ctr P30-33	21.97 ± 4.91	7/3	1.23 ± SEM (+0.10; −0.10)	8/3
sh95 P30-33	46.78 ± 4.76	8/3	0.82 ± SEM (+0.10; −0.09)	8/3
ctr P60-70	0.85 ± 2.24	7/4	1.90 ± SEM (+0.15; −0.14)	17/6
sh95 P60-70	44.72 ± 1.76	7/4	1.06 ± SEM (+0.14; −0.12)	11/3
GFP P60-70			1.90 ± SEM (+0.17; −0.16)	19/5
ctr P80-90			2.28 ± SEM (+0.45; −0.38)	6/3
sh95 P80-90			1.13 ± SEM (+0.17; −0.15)	8/3

Table S3. Protein levels for adult WT and PSD-95 KO mice of Fig. 3

	Band signal intensity	
Protein	WT	KO
GluA1	1.00 ± 0.10	0.51 ± 0.09
GluA2	1.00 ± 0.09	0.33 ± 0.02
GluA3	1.00 ± 0.06	0.57 ± 0.04
GluA4	1.00 ± 0.05	0.90 ± 0.04
GluN2A	1.00 ± 0.07	0.92 ± 0.14
GluN2B	1.00 ± 0.05	1.03 ± 0.12
$GABA_AR$-α1	1.00 ± 0.16	0.94 ± 0.16
Gephyrin	1.00 ± 0.19	0.87 ± 0.08

Table S4. AMPA/NMDA and GABA/NMDA ratios of Fig. 4

Group	AMPA/NMDA ratio	GABA/NMDA ratio	Cells per mice
WT P30	0.80 ± SEM (+0.04; −0.04)	2.12 ± SEM (+0.26; −0.23)	16/4
KO P30	0.62 ± SEM (+0.10; −0.08)	2.01 ± SEM (+0.06; −0.05)	17/3
WT P60	1.22 ± SEM (+0.13; −0.12)	3.77 ± SEM (+0.37; −0.34)	16/4
KO P60	0.67 ± SEM (+0.08; −0.07)	3.65 ± SEM (+0.46; −0.41)	14/3
PV+ interneurons			
WT P60	8.77 ± SEM (+0.43; −0.41)		15/3
KO P60	8.90 ± SEM (+0.84; −0.77)		16/3